2014 IEEE International Conference on Robotics & Automation (ICRA)
Hong Kong Convention and Exhibition Center
May 31 - June 7, 2014. Hong Kong, China

Active Microrheology of the Vitreous of the Eye applied to Nanorobot Propulsion*

Tian Qiu, Debora Schamel, Andrew G. Mark, and Peer Fischer, *Member, IEEE*

***Abstract*— Biomedical applications of micro or nanorobots require active movement through complex biological fluids. These are generally non-Newtonian (viscoelastic) fluids that are characterized by complicated networks of macromolecules that have size-dependent rheological properties. It has been suggested that an untethered microrobot could assist in retinal surgical procedures. To do this it must navigate the vitreous humor, a hydrated double network of collagen fibrils and high molecular-weight, polyanionic hyaluronan macromolecules. Here, we examine the characteristic size that potential robots must have to traverse vitreous relatively unhindered. We have constructed magnetic tweezers that provide a large gradient of up to 320 T/m to pull sub-micron paramagnetic beads through biological fluids. A novel two-step electrical discharge machining (EDM) approach is used to construct the tips of the magnetic tweezers with a resolution of 30 μm and high aspect ratio of ~17:1 that restricts the magnetic field gradient to the plane of observation. We report measurements on porcine vitreous. In agreement with structural data and passive Brownian diffusion studies we find that the unhindered active propulsion through the eye calls for nanorobots with cross-sections of less than 500 nm.**

I. Introduction

The human body contains a variety of complex biological fluids. They are often non-Newtonian fluids with viscoelastic properties, [1] *e.g.* mucus, sputum, vitreous humor of the eye, *etc.* Many of them, *e.g.* blood, saliva, and synovial fluid in the joints, exhibit shear thinning behavior. Understanding the local rheology is necessary if micro and nanorobots are to navigate these complex fluids. A number of micro-robots have been realized that swim in Newtonian fluids [2-5], but the movement in a non-Newtonian fluid poses extra challenges. There is a need to understand the local rheology of these biologically and medically important fluids down to the nanoscale in order to optimize the design of nanorobots and artificial micro-swimmers.

In microrheology, colloidal particles are directly embedded in the fluid, which permits its rheological characterization at small length scales. [6] This approach has several advantages over traditional rheological measurements. Only small sample volumes down to microliters are required [7]. Secondly, due to small size of the probe, microrheology is able to provide local information in inhomogeneous media. In passive microrheology, the random movements of colloidal probes by thermal excitation are measured to very high frequencies, far beyond those possible in macroscopic rheometry; while in active microrheology the interaction of micro probes with the microstructure is directly measured and local material heterogeneities can be analyzed [6]. Last but not least, micro probes can be injected into real biological tissues, even *in vivo*. This is extremely important for biomedical samples, for which the fluidic properties may change dramatically due to degradation, liquidation *etc.* after removal to an *ex situ* environment.

Active microrheology probes have been actuated by different approaches, including optical tweezers, magnetic tweezers and atomic force microscopes (AFM).[8] Among these, magnetic tweezers [9-12] exert the largest force on the probe. In previous work, different geometries have been proposed for magnetic tweezers, depending on the number of magnetic poles. [13, 14] Key in all setups is the number, shape and size of the magnetic pole tips. These should be very thin in the horizontal direction in order to realize a high gradient, but stay in well-defined relative positions. Pole tips are generally made by electroplating [13], pulsed electrodeposition followed by photolithography[15] or laser cutting [14]. The drawback with these approaches is that they cannot fabricate large heights of the magnetic layer (the largest height is normally smaller than 10 μm by deposition or plating and smaller than 200 μm by laser cutting), which may lead to an inhomogeneous magnetic field orthogonal to the viewing direction (Z-height in a microscope). Any unwanted Z-component of the gradient will drag the magnetic beads out of the focus plane of the microscope and severely limit the accuracy of the microrheological measurements. Another disadvantage of electroplating or vapor deposition processes is the difficulty in exercising the stoichometric control necessary for advanced magnetic alloys.

Here, we describe a three-pole magnetic tweezer whose tips are fabricated by electrical discharge machining (EDM). The EDM method can process tips with deep sections (500 μm thickness or more), high spatial resolution (30 μm) with high aspect ratio (thickness *vs*. tip apex diameter ~17:1). The three tips produce a large and homogeneous magnetic field gradient. The gradient is characterized by applying Stokes law to magnetic beads dragged through a Newtonian fluid. We apply this instrument to measure the rheological properties, under active manipulation, of vitreous humor, a target medium for biomedical robots. The measurements show that the mesh of the polymer network found in the vitreous impedes the

* This work was supported by the Max Planck Society and the European Research Council under the ERC Grant agreement Chiral MicroBots (278213).

T. Qiu, D. Schamel, A. G. Mark and P. Fischer are with Max Planck Institute for Intelligent Systems, 70569 Stuttgart, Germany (corresponding author: P. Fischer; +49 711 689-3560; e-mail: fischer@is.mpg.de).

T. Qiu is also with Institute of Bioengineering, Ecole Polytechnique Fédérale de Lausanne (EPFL), CH-1015 Lausanne, Switzerland.

D. Schamel and P. Fischer are also with the Institut für Physikalische Chemie, Universität Stuttgart, Pfaffenwaldring 55, 70569 Stuttgart, Germany.

passage of particles greater than 500 nm in diameter. This establishes an important size constraint for nanorobots intended to operate freely within the eye.

II. Materials and Methods

A. Materials and sample preparation

Four kinds of paramagnetic beads were used. 0.5 µm, 1.0 µm and 1.89 µm diameter magnetic beads (PMSi-CH.5-5, PMSi-CH1.0-5, PMC-1.5, respectively, all with carboxyl functional groups, 25 mg/mL) were obtained from Kisker Biotech. Larger 2.7 µm diameter magnetic beads (Dynabeads M-270, Amine functional group, $2x10^9$ beads/mL) were obtained from Invitrogen.

500 µL of glycerol (99.5%, VWR), used as received, was mixed thoroughly with 5 µL of 0.5 or 1.0 µm diameter beads with quantum dot coupling, or 1 µL of 1.89 µm diameter beads without quantum dot coupling.

Porcine eyes were kept on ice and experiments were carried out within 6 h of harvesting. The vitreous from the eye was dissected with a scalpel. The dissected ~1 mm3 parts were randomly selected for the microrheology study, and injected with 2 µL of beads (with diameters of, respectively, 0.5 µm, 1.0 µm and 2.7 µm).

B. Quantum dot coupling to the magnetic beads

250 µL of carboxyl-functionalized superparamagnetic silica particles (0.5 and 1 µm diameter) were mixed with 750 µL MES-buffer pH 6.5 (final concentration 20 mM). 2 mg of 1-ethyl-3-(3-dimethylaminopropyl) carbodiimid (EDC; Sigma Aldrich) and 1 mg of N-Hydroxysuccinimid (NHS; Sigma Aldrich) were added and the mixture was stirred for 2 h at 4 °C. The particles were washed twice with MES-buffer by centrifugation and resuspension, and dispersed in 0.5 mL MES-buffer (pH 6.5, 20 mM) containing 2 µL of amino-functionalized eFluor 650NC (eBioscience). The solution was stirred over night at 4 °C and washed 3 times with water by centrifugation.

C. Magnetic tweezers apparatus

As illustrated in Fig. 1, the magnetic tweezers apparatus uses a 3-pole geometry to achieve 2D control of the micro-probes in the plane of the tips. Three independently driven coils control the magnetic field in each tip. Each coil is made of 2200 turns of 0.5 mm diameter copper wire around a steel spool (St 37-2). A thermocouple embedded in the middle of each coil monitors its temperature (Fig. 1(B)).

The three pole tips are the key elements of the apparatus. From the outer circumference of the apparatus where they connect to the coils, each pole tip tapers to a fine apex. The three tips, arranged at 120°, point inwards towards the working volume. To achieve high gradients the apices need to be closely spaced, and in order to maintain a symmetric field within the working volume requires high spatial precision, and long-term stability. However, efficient control of the magnetic flux requires that each tip is isolated from the others by areas of high magnetic reluctance. These requirements – separated micro-sized tips keeping precise relative positions at micro-scale range – place stringent demands on the manufacturing process.

A novel 2-step EDM approach was used to achieve the manufacturing requirements of the tips. The process is shown in detail in Fig. 2. First, a 500 µm thick steel plate (St37-2) was cut by wire EDM. The final arrangement of the three tip apices is established in this step. They remain temporarily connected by a ring around the outer circumference that fixes their relative positions, as shown in Fig. 2(A). The EDM wire diameter determines the minimum apex spacing, shown in Fig. 1(C). We have achieved spacings as small as 220 µm, with tip diameters smaller than 30 µm. EDM is appropriate for cutting any conductive material, including pure metals or alloys, it can cut thick sheets, and the technique is quick and cost effective.

In the second step (Fig. 2(B)), screws are used to mount the steel plate to an aluminum frame. The three tips are further secured with an epoxy stabilizing ring (green) that is cast to shape in a PDMS (polydimethylsiloxane) mold. The central hole in the ring leaves the three tip apecies exposed and allows access to the working volume. Its diameter can be varied from 300 µm to several mm for different applications.

Next, a second EDM cut removes the sacrificial ring joining the three tips. This step eliminates the unwanted low reluctance path between the tips (Fig. 2(C)). During this operation, the epoxy and screws fix the tips and prevent relative motion between them. Comparing the SEM pictures before (Fig. 3(A) corresponding to Fig. 2(B)) and after (Fig. 3(B) corresponding to Fig. 2(C)) the second EDM cut, no significant changes of positions or shapes are observed. Finally, the three drive coils and a steel pole piece are assembled above the tips (Fig. 3(D)).

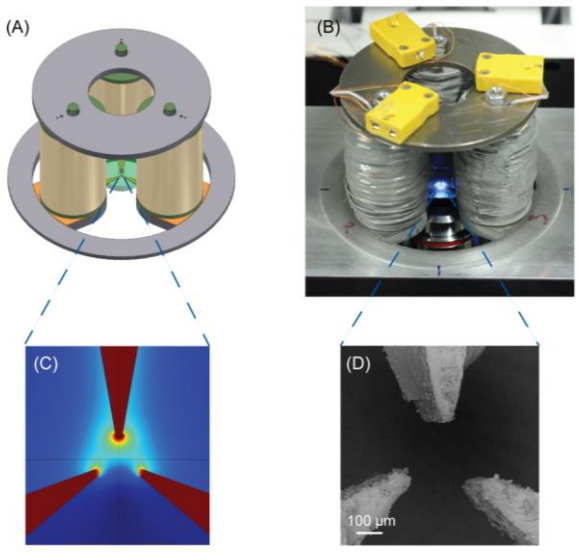

Figure 1. Magnetic tweezers apparatus. (A) 3D design model of the apparatus. (B) picture of the assembled apparatus on the microscope stage. (C) Enlarged picture of the three pole tips. Calculated magnetic field flux density is shown by color map. (D) Scanning electron microscope (SEM) image of the three pole tips at a viewing angle of 10 degrees.

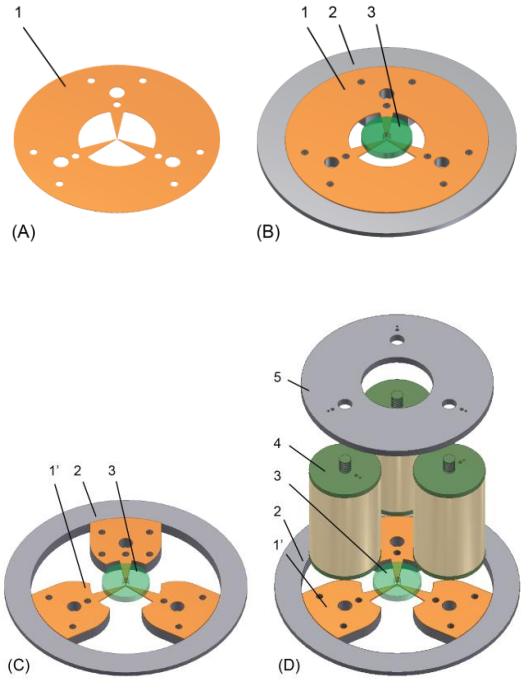

Figure 2. Manufacturing process of the apparatus. (A) First EDM cut of the steel plate. (B) Steel plate mounted to the aluminum holder. Epoxy is cured in the central area but leaving the three tips exposed. (C) Second cut of the steel plate. (D) Assembly of the apparatus. The numbers represent 1- steel plate after first EDM cut, 1'- steel plate after second EDM cut, 2- aluminum frame, 3- epoxy, 4- coil, 5- top pole piece.

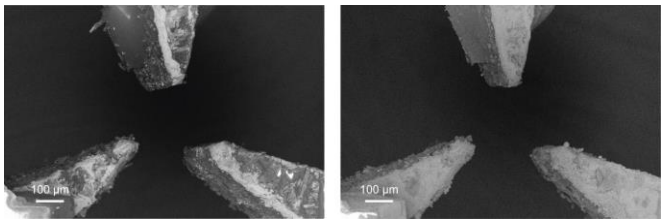

Figure 3. SEM images of the three pole tips before (A) and after (B) the second EDM cut show no changes in position or shape.

D. Magnetic field simulation

A 3D model of the apparatus was created in Inventor 2012 (Autodesk Inc.) and the magnetic performance was simulated in Comsol 4.3 (Comsol Multiphysics). Because the feature sizes of the tips (30 µm) and coils (30 mm) differ by three orders of magnitude, the model was simulated in two separate parts: the coil and the three tips. This allowed finer resolution of the mesh at the pole tips, without requiring micron scale mesh sizes over the entire apparatus volume. The magnetic flux generated by the coil in the large-scale calculation was applied as a magnetization to the tips in the small scale model. In this manner the magnetic field in the working volume between the three tips was simulated.

E. Magnetic gradient calibration

We used measurements of magnetic particle velocity in a Newtonian fluid to calibrate the magnetic gradient using Stokes law. The fluid drag F of a sphere moving at low Reynolds number is:

$$F = 6\pi\eta \mathrm{R} v \tag{1}$$

where η is the viscosity of the fluid, R is the radius of the sphere, and v is the velocity of the sphere.

The magnetic force F on an object whose magnetic moment M is aligned with the magnetic field is

$$F = \mathrm{M} \cdot \nabla \mathrm{B} \tag{2}$$

where B is the magnitude of the magnetic field. For a homogeneous particle, the magnetic moment is

$$M = H_{\mathrm{ci}} \ \mathrm{V} \tag{3}$$

For the magnetic beads used here $H_{\mathrm{ci}} = 3.5 \times 10^5 \ A/m$ [16]. V is the volume of the object, which in this case

$$\mathrm{V} = \frac{4}{3}\pi \mathrm{R}^3 \tag{4}$$

With known properties of the magnetic beads, we measure the velocity of the beads v to calculate the gradient of the field $\nabla \mathrm{B}$ from equations (1) and (4):

$$\nabla \mathrm{B} = \frac{9\eta v}{2R^2 H_{ci}} \tag{5}$$

Furthermore, it can be seen that for a given gradient, the relationship between the beads' velocity v and diameter d is quadratic:

$$v = \frac{H_{ci} \nabla \mathrm{B}}{18\eta} d^2 \tag{6}$$

F. Microrheology measurement

Prepared fluid was added to the sample hole among the three tips where it was held by surface tension. A DC current generated by a programmable amplifier was applied to one coil, while the other two coils remained inactivate. The movement of the magnetic probes was observed by an inverted microscope under 50x objective (NA=0.55, Zeiss). For beads smaller than 1 µm, 650 nm fluorescence was detected (an additional long pass filter 605 nm before the CCD to filter the fluorescence of the epoxy stabilizing ring); for beads larger than 1 µm bright field was used. The video was recorded at 5 frames/s, particle velocities were analyzed in ImageJ (NIH), and the trajectories were drawn by the Mosaic plugin [17].

In glycerol, 3 sizes of beads, 0.5, 1.0, 1.89 µm, were tested at a constant current of 0.25 A. For 1.0 µm beads, four different currents, 0.25, 0.5, 1.0, 2.0 A were applied. In porcine vitreous, three sizes of beads, 0.5, 1.0, 2.7 µm, were tested at a constant current of 0.5 A.

III. Results and Discussions

A. Simulation results

The results of the simulations of the magnetic flux density on the center plane of the tips, with 2.0 A excitation current, are shown in Fig. 4(A) and (B). The strength and gradient along the three principal axes running through the center point are shown in Fig. 4(C). The magnetic flux density increases dramatically from 0.1 T to 1.0 T within the 300 µm gap. The highest gradient is achieved very near the tips, however this area is not useful for microrheology, because the gradient there is non-uniform (*i.e.* the second derivative of the field strength is non-negligible) and particles will also be easily attracted to and trapped by the tip. In contrast, inside the working volume, 50 µm from the center point, the field gradient in the x-direction is almost constant at ~1 kT/m, ideal for microrheology experiments. Furthermore, the gradients in the y and z directions are negligible.

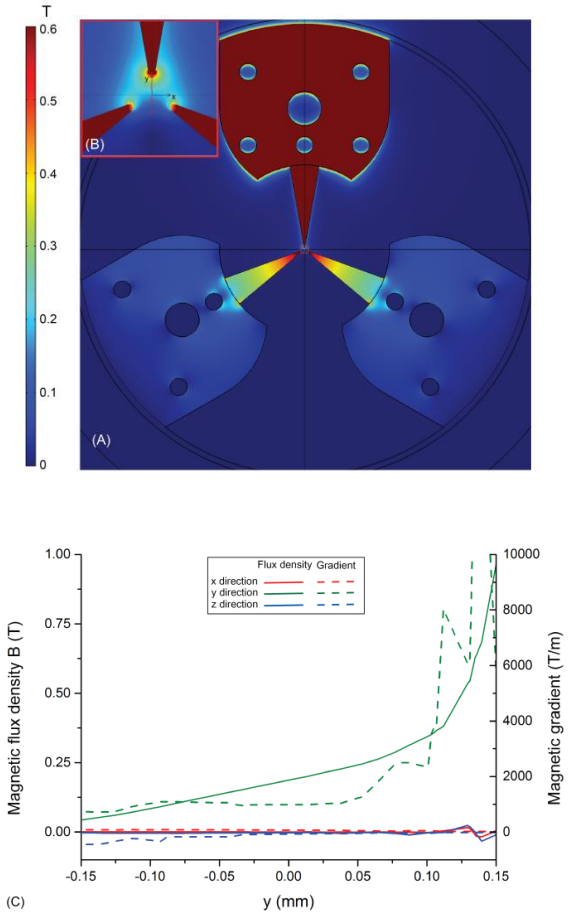

Figure 4. Comsol simulation results of the magnetic field. (A) Magnetic flux density. (B) Enlarged picture of the central tip area (shown as red box in A). x and y directions are shown by arrows. (C) The magnetic flux density and gradient along the center line (shown as red dashed line in B).

B. Magnetic gradient calibration

To measure the magnetic gradient, we used different beads in glycerol of known viscosity. All experiments were conducted with a constant current of 0.25 A. As shown in Fig. 5(A), the velocity of beads increases quadratically with diameter, in accord with equation (6). Since the magnetic force rises with the cube of bead's diameter, while the fluidic drag increases only linearly, in a Newtonian fluid larger particles move faster. However, as we shall see, this may not be true if the fluid is non-Newtonian, especially if it contains complicated networks *e.g.* a biopolymer network.

The gradient's response to coil current was tested with 1.0 µm beads. As expected, the bead velocity, and hence the field gradient driving them, rises linearly with the current (Fig 5(B)). The measured gradient at 2.0 A current is 320±74 T/m. This is about 3 times smaller than the simulation result. The discrepancy arises because the simulation was conducted on separate coil and tip models matched by the flux injected into the tip. This likely overestimates the magnetization of the tip. Secondly, at this field the steel tips have already reached saturation near their apices. The saturation flux density of St37-2 steel is about 1.5 T,[18] smaller than the largest flux density found in the simulation. The gradient could be further improved by using a material with a higher saturation magnetization. For example oriented silicon iron saturates at 2.0 T [19] and would therefore provide a maximum gradient 1.3 times higher than the current material.

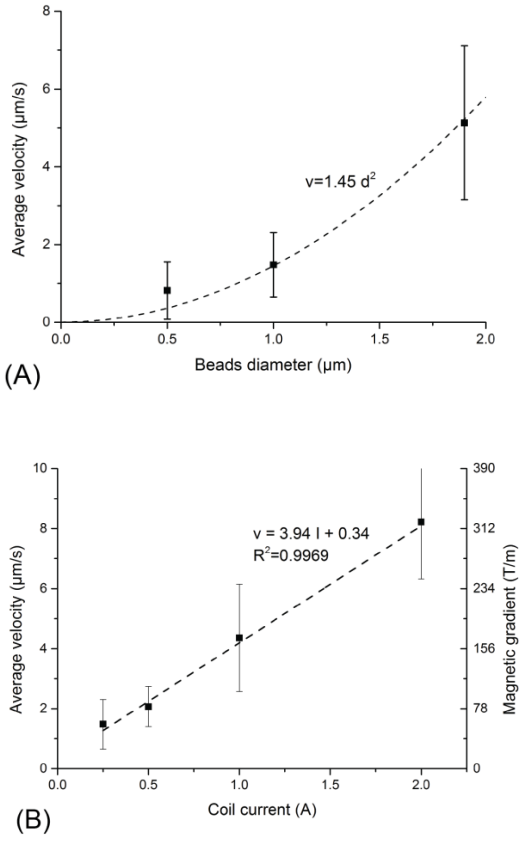

Figure 5. Magnetic gradient characterization in glycerol. (A) Beads' average velocity increases quadratically with diameter at fixed coil current 0.25 A. The dashed line is the quadratic fit of the data. (B) Beads' average velocity increases linearly with coil current at fixed bead diameter 1.0 µm. Magnetic gradient strengths are calculated based on Eqn. (5).

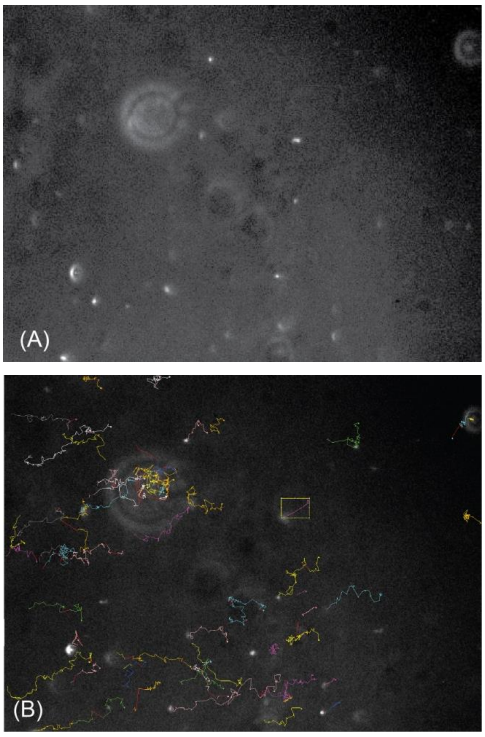

Figure 6. 500 nm diameter magnetic beads in porcine vitreous and the corresponding tracking trajectories. (A) Fluorescent image taken under microscope. (B) Tracking trajectories of the beads along gradient towards top right corner. See also supplementary movie S1.

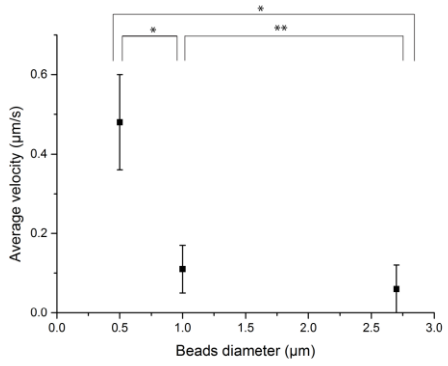

Figure 7. Average velocities of different diameter beads in the porcine vitreous (*t*-test * P<0.001, ** P>0.05).

C. *Active microrheology measurements of vitreous*

Fig. 6(A) shows the fluorescent image of 500 nm diameter magnetic beads in porcine vitreous. As the trajectories in Fig. 6(B) and supplementary movie S1 show, the beads are actively pulled by the magnetic gradient through the vitreous. The average linear velocity was 0.48±0.12 μm/s for a gradient of ~80 T/m. This indicates that the porcine vitreous has an apparent viscosity of 0.8 Pa•s to 500nm beads according to equation (5).

However, 1.0 μm beads under the same gradient moved at a velocity of 0.11±0.06 μm/s, significantly lower than the 500 nm ones (P<0.001 for *t*-test). Similarly, 2.7 μm beads for the same gradient (0.06±0.06 μm/s) were almost immobile, which shows no significant difference with 1.0 μm beads (P>0.05 for *t*-test). In contrast, for a Newtonian fluid one would expect that the velocity of beads should increase quadratically with the bead diameter (shown in Fig. 5(A)). The reason is the underlying complexity of the vitreous which is composed of a polymer network of collagen type II fibrils and high molecular-weight, polyanionic hyaluronan macromolecules [20]. It follows that if the particle diameter is smaller than the mesh size, it can easily be pulled through the vitreous.

A previous study of passive Brownian diffusion and structural data shows that the mesh size of bovine vitreous is ~550±50 nm, and polystyrene nanoparticles coated with –COOH in the size range of 100-200 nm readily diffused through the mesh.[21] Our data agrees with this result, moreover, we find that 500 nm –COOH coated nanoparticles can be actively pulled through the polymer network. In this paper high magnetic gradients were used to achieve active pulling of the nanoparticles. It will be of interest to determine the smallest practical gradients that can be used to pull nanoparticles through the vitreous, and in particular if such a scheme can be realized *in vivo*. Active actuation of the nanoparticles provides more potential for targeted drug delivery to specific region. Moreover, finding the largest possible size that can actively pass through the polymer network provides useful information for the design of untethered nanorobots moving through complex biological tissues.

IV. Conclusions

In this work, we report a novel two-step EDM approach to manufacture magnetic tweezer tips at high horizontal resolution (30 μm) and high aspect ratio (~17:1). This is a fast and cost-effective method to construct high gradient magnetic tweezers (320 T/m) with a homogeneous direction that restricts the gradient to the plane of observation. This system was utilized to study the microrhelogy of porcine vitreous. We discovered that unhindered active propulsion through the eye calls for nanorobots with cross-sections of less than 500 nm. This system has the potential to be a reliable and easy-to-use method to study the microrheolgy of biological fluids and provide useful information on the design of artificial self-propelling and untethered micro-robots in complex biofluids.

References

[1] Y. C. Fung, "Bio-viscoelastic Fluids," in *Biomechanics*, 1981, pp. 174-195.

[2] A. Ghosh and P. Fischer, "Controlled Propulsion of Artificial Magnetic Nanostructured Propellers," *Nano Letters,* vol. 9, pp. 2243-2245, Jun 2009.

[3] D. Schamel*, et al.*, "Chiral Colloidal Molecules And Observation of The Propeller Effect," *Journal of the American Chemical Society,* doi: 10.1021/ja405705x, 2013.

[4] L. Zhang*, et al.*, "Artificial bacterial flagella: Fabrication and magnetic control," *Applied Physics Letters,* vol. 94, p. 064107, Feb 2009.

[5] S. Tottori*, et al.*, "Magnetic Helical Micromachines: Fabrication, Controlled Swimming, and Cargo Transport," *Advanced Materials,* vol. 24, pp. 811-816, Feb 2012.

[6] T. M. Squires and T. G. Mason, "Fluid Mechanics of Microrheology," *Annual Review of Fluid Mechanics,* vol. 42, pp. 413-438, 2010.

[7] D. Weihs, *et al.*, "Bio-microrheology: A frontier in microrheology," *Biophysical Journal,* vol. 91, pp. 4296-4305, Dec 2006.
[8] K. C. Neuman and A. Nagy, "Single-molecule force spectroscopy: optical tweezers, magnetic tweezers and atomic force microscopy," *Nature Methods,* vol. 5, pp. 491-505, Jun 2008.
[9] F. Ziemann, *et al.*, "Local Measurements of Viscoelastic Moduli of Entangled Actin Networks Using an Oscillating Magnetic Bead Micro-Rheometer," *Biophysical Journal,* vol. 66, pp. 2210-2216, Jun 1994.
[10] A. R. Bausch, *et al.*, "Measurement of local viscoelasticity and forces in living cells by magnetic tweezers," *Biophysical Journal,* vol. 76, pp. 573-579, Jan 1999.
[11] M. Keller, *et al.*, "Oscillatory magnetic bead rheometer for complex fluid microrheometry," *Review of Scientific Instruments,* vol. 72, pp. 3626-3634, Sep 2001.
[12] J. Pokki, *et al.*, "Localized viscoelasticity measurements with untethered intravitreal microrobots," *Conf Proc IEEE Eng Med Biol Soc,* vol. 2012, pp. 2813-2816, 2012.
[13] A. H. B. de Vries, *et al.*, "Micro magnetic tweezers for nanomanipulation inside live cells," *Biophysical Journal,* vol. 88, pp. 2137-2144, Mar 2005.
[14] J. K. Fisher, *et al.*, "Thin-foil magnetic force system for high-numerical-aperture microscopy," *Review of Scientific Instruments,* vol. 77, p. 023702, Feb 2006.
[15] P. T. Tang, "Pulse reversal plating of nickel and nickel alloys for microgalvanics," *Electrochimica Acta,* vol. 47, pp. 61-66, Sep 2001.
[16] G. Fonnum, *et al.*, "Characterisation of Dynabeads (R) by magnetization measurements and Mossbauer spectroscopy," *Journal of Magnetism and Magnetic Materials,* vol. 293, pp. 41-47, May 2005.
[17] I. F. Sbalzarini and P. Koumoutsakos, "Feature point tracking and trajectory analysis for video imaging in cell biology," *Journal of Structural Biology,* vol. 151, pp. 182-195, Aug 2005.
[18] S. Sgobba, "Physics and measurements of magnetic materials," *CERN,* vol. 4, pp. 39-63, 2010.
[19] D. Benjamin, *Metals Handbook: Properties and Selection: Stainless Steels, Tool Materials and Special-Purpose Metals*, 9th ed. vol. 3: American Society for Metals, 1980.
[20] P. N. Bishop, "Structural macromolecules and supramolecular organisation of the vitreous gel," *Progress in Retinal and Eye Research,* vol. 19, pp. 323-344, May 2000.
[21] Q. G. Xu, *et al.*, "Nanoparticle diffusion in, and microrheology of, the bovine vitreous ex vivo," *Journal of Controlled Release,* vol. 167, pp. 76-84, Apr 10 2013.